1-10-1992

Late Holocene Tectonics and Paleoseismicity, Southern Cascadia Subduction Zone

Samuel H. Clarke Jr.

Gary A. Carver

1-10-1992

Late Holocene Tectonics and Paleoseismicity, Southern Cascadia Subduction Zone

Samuel H. Clarke Jr.

Gary A. Carver

a picture of the bonding at different levels in the reconstruction.

On the basis of the data in Fig. 1B, the Ge(111) surface consists of an outer adatom layer and a rest-layer that has a bulk (1 × 1) structure. The backbonds that bind these adatoms to the rest-layer are known to be highly strained (*11*). After reaction with the dangling surface bonds, hydrogen proceeds to attack these strained backbonds, which results in bond scission. Hydrogen reacts with the dangling bonds generated by this bond scission, thus stabilizing the (1 × 1) bulk rest-layer structure and hydrogenating the adatom species. Further reaction with this adatom species results in further backbond scission and hydrogenation, and ultimately GeH_4 formation. In this manner, the adatoms are removed and the underlying rest-layer is exposed. However, not all of the adatoms react in this manner. Hydrogen also facilitates the formation of hydrogenated adatom islands on the surface. This is an alternative mechanism to relieve the strain in the backbonds and results in the formation of islands with largely relaxed Ge–Ge bonds. Similar mechanisms were observed on the Si(111)-(7 × 7) surface (*9, 12, 13*). In each case, these reactions serve to expose the underlying rest-layer and allow it to be directly imaged by the STM. On the other hand, reaction of the unstrained rest-layer bonds is very slow and is not observed under the present conditions. In addition to the larger barrier associated with this reaction, the compact (111) structure limits the ability of hydrogen to penetrate the surface (*14*).

This technique is not limited to Ge surfaces; the structure of the Si(111)-(7 × 7) surface can be probed in a similar manner (*9, 12, 13*). The Si(111) surface also has an adatom surface layer but the rest-layer beneath has a nonbulk structure consisting of triangular subunits bounded by rows of dimers (*6*). As in the case of the Ge(111) surface, reaction at room temperature exposes the rest-layer through SiH_4 and adatom island formation. The moderately strained dimer bonds do not react under these conditions. However, by annealing or dosing at 550 K the dimer bonds gradually react and the rest-layer slowly adopts a bulk-like structure. The elevated reaction temperature is a reflection of the moderate strain associated with these dimer bonds and a correspondingly larger barrier to reaction (see Fig. 2). Here too the reactivity is controlled by bond strain, allowing hydrogen to sequentially react with, and effectively titrate, the different surface bonds.

Although the presence of this strain field is an intrinsic property of covalent semiconductor materials, not all adsorbates serve as useful probes of surface structure. The ideal adsorbate must be monovalent and form strong bonds with semiconductors so that the adsorbate can saturate the dangling bonds produced by bond scission and stabilize the exposed surface. The adsorbate should be small to avoid interadsorbate interactions and to penetrate the surface structure. Most importantly, however, the adsorbate must show selectivity between bonds with different degrees of strain. It is this characteristic that allows hydrogen to pick apart the reconstruction. Chlorine fails in this regard; both the backbond and dimer-bond reactions on the Si(111) surface proceed effectively only at elevated temperatures (*15, 16*). Bromine, however, is too large, and fluorine reactions are so exothermic that little selectivity is expected. This selectivity, together with the ability to react with and stabilize the dangling bonds of the exposed layer, makes hydrogen an effective chemical probe of surface structure.

REFERENCES AND NOTES

1. D. Haneman, *Rep. Prog. Phys.* **50**, 1045 (1987).
2. G. Binnig and H. Rohrer, *Helv. Phys. Acta.* **55**, 726 (1982).
3. R. S. Becker, B. S. Swartzentruber, J. S. Vickers, T. Klitsner, *Phys. Rev. B* **39**, 1633 (1989).
4. R. M. Feenstra and A. J. Slavin, *Surf. Sci.* **251/252**, 401 (1991).
5. E. S. Hirschorn, D. S. Lin, F. M. Leibsle, A. Samsavar, T.-C. Chiang, *Phys. Rev. B* **44**, 1403 (1991).
6. K. Takayanagi, Y. Tanishiro, M. Takahashi, S. Takahashi, *J. Vac. Sci. Technol. A* **3**, 1502 (1985).
7. Y. G. Hao and L. M. Roth, *Surf. Sci.* **232**, L201 (1990).
8. J. E. Demuth, R. J. Hamers, R. M. Tromp, M. E. Welland, *J. Vac. Sci. Technol. A* **4**, 1320 (1986).
9. J. J. Boland, *Surf. Sci.* **244**, 1 (1991).
10. I. Ohdamari, *ibid.* **227**, L129 (1990).
11. R. D. Meade and D. Vanderbilt, *Phys. Rev. B* **40**, 3905 (1989).
12. J. J. Boland, *J. Phys. Chem.* **95**, 1521 (1991).
13. ———, *J. Vac. Sci. Technol. B* **9**, 764 (1991).
14. ———, *Surf. Sci.* **261**, 17 (1992).
15. J. S. Villarrubia and J. J. Boland, *Phys. Rev. Lett.* **63**, 306 (1989).
16. J. J. Boland and J. S. Villarrubia, *Phys. Rev. B* **41**, 9865 (1990).

1 October 1991; accepted 31 October 1991

Late Holocene Tectonics and Paleoseismicity, Southern Cascadia Subduction Zone

SAMUEL H. CLARKE, JR., AND GARY A. CARVER

Holocene deformation indicative of large subduction-zone earthquakes has occurred on two large thrust fault systems in the Humboldt Bay region of northern California. Displaced stratigraphic markers record three offsets of 5 to 7 meters each on the Little Salmon fault during the past 1700 years. Smaller and less frequent Holocene displacements have occurred in the Mad River fault zone. Elsewhere, as many as five episodes of sudden subsidence of marsh peats and fossil forests and uplift of marine terraces are recorded. Carbon-14 dates suggest that the faulting, subsidence, and uplift events were synchronous. Relations between magnitude and various fault-offset parameters indicate that earthquakes accompanying displacements on the Little Salmon fault had magnitudes of at least 7.6 to 7.8. More likely this faulting accompanied rupture of the boundary between the Gorda and North American plates, and magnitudes were about 8.4 or greater.

THE POTENTIAL FOR LARGE EARTHquakes along the Cascadia subduction zone (CSZ) has been controversial; some (*1*) have interpreted crustal deformation data and the absence of large magnitude thrust earthquakes during the last 150 years to indicate that plate convergence averaging 30 to 40 mm/yr (*2*) is accommodated by aseismic slip. Others (*2*) have noted that the lack of large magnitude subduction-related earthquakes, the young age of the subducted plate, the shallow dip of the subduction zone (10° to 15°), and the subdued offshore trench are consistent with strong coupling between the plates, and suggest that the CSZ is capable of producing great magnitude [$M_w > 8.5$; (*3*)] earthquakes.

The southern Cascadia subduction zone (SCSZ) and overlying accretionary prism lie partly offshore, but also extend onland in northern California (Fig. 1) (*4, 5*). As a result examination of the offshore structure of the subduction margin by acoustic-reflection techniques (*4, 6*) can be integrated with paleoseismic studies on land. In this report, we use dated fault displacements together with evidence of coincident coseismic uplift and subsidence to evaluate the Holocene seismic activity and earthquake potential of the SCSZ.

The accretionary prism of the SCSZ is 85 to 100 km wide and comprises prominent systems of north-northwest trending, east-

S. H. Clarke, Jr., Branch of Pacific Marine Geology, U.S. Geological Survey, 345 Middlefield Road, Mail Stop 999, Menlo Park, CA 94025.
G. A. Carver, Department of Geology, Humboldt State University, Arcata, CA 95521.

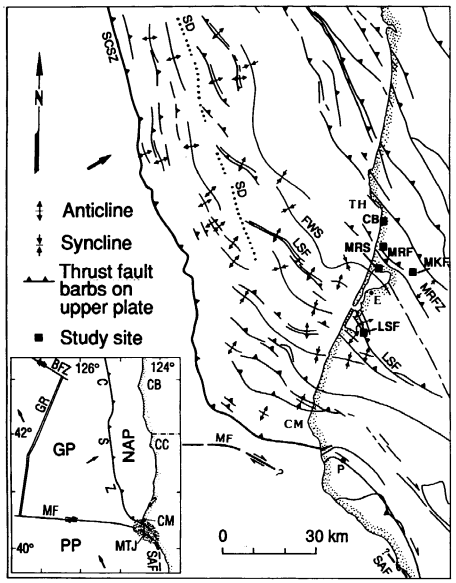

Fig. 1. Plate tectonic setting of the northwestern California continental margin. Arrows indicate oceanic-plate motions relative to North American plate. Barbed line shows the base of the continental slope, the approximate boundary between the Gorda (GP) and North American (NAP) plates. Half arrows on inset map indicate relative motions along the Blanco fracture zone (BFZ) and the Mendocino fault (MF). Other abbreviations are: locations: CB, Cape Blanco; CC, Crescent City; CM, Cape Mendocino; E, Eureka; P, Petrolia; and TH, Trinidad Head. Structural features: CSZ, Cascadia subduction zone; GR, Gorda Ridge; LSF, Little Salmon fault; MRFZ, Mad River fault zone; MTJ, area of Mendocino triple junction; SAF, San Andreas fault; SCSZ, Southern Cascadia subduction zone; PP, Pacific Plate; and SD (heavy dotted line), structural discontinuity mentioned in text. Study sites: CB, Clam Beach; LSF, Little Salmon fault; MKF, McKinleyville fault; MRF, Mad River fault; and MRS, Mad River Slough.

northeast dipping en echelon thrust faults, fault-related anticlines, and broad open synclines (Fig. 1) (7). This contractional domain is buttressed on the east by the Klamath Mountains. A structural discontinuity located 15 to 25 km east of the SCSZ deformation front separates north- to northwest trending structures to the west from northwest trending ones to the east (SD in Fig. 1) (7). This discontinuity forms the approximate western limit of seismicity on the North American plate (*8*). In the southern part of the region, structures take on a west to northwest trend and extend landward (Fig. 1).

Faults of the SCSZ fold-and-thrust belt form two or more west-verging imbricate thrust fans (Fig. 1) (*5, 7*). Deep penetration seismic-reflection surveys offshore show that these fans merge into sole thrust faults that extend to or near (~4 to 5.5 km above) the interface between the Gorda and North American plates (7). Individual faults commonly extend upward to or near the sea floor and terminate in folds that deform young strata. Onland, cumulative slip greater than 15 km has been estimated from measured vertical separations of lower Pleistocene sediments across faults (*5, 9*). These relations and displacements of upper Pleistocene marine terraces (*5, 10, 11*) indicate that the average rate of shortening across the belt since this time is ≥20 mm/yr.

First motions of earthquakes on the North American plate north of the Mendocino triple junction (MTJ) (*8*) and interpretations from geodetic (*12*) and borehole breakout (*13*) data are also consistent with northeast-directed compression. This compression is nearly parallel to the convergence vector between the Gorda and North American plates (Fig. 1) (*12*), and accommodates more than half of the overall plate convergence (*14–16*). The shortening associated with growth of the fold-and-thrust belt together with the obvious youth of the structures implies that coupling across the subduction zone is strong and that convergence-related compressive deformation of the North American plate margin is active. Such interplate coupling is compatible with the buoyancy of the young Gorda plate (<6 Ma) where it enters the SCSZ. This evidence is bolstered by acoustic-reflection profiles that show clear evidence of compressive deformation and incipient thrust faulting in Pliocene and younger cover sediments in the Gorda basin along the western edge of the SCSZ [figure 7 in (7)].

Holocene sediments and landforms in the Humboldt Bay region record deformation resulting from sudden slip on several major thrust faults, sudden uplift of sections of the coast north of the MTJ, and sudden subsidence of the axis of a prominent fold, the Freshwater syncline (Fig. 1) (*17–19*). Trenches across three principal thrust faults have exposed sequences of deformed sediments from which we have interpreted Holocene paleoseismicity (*17, 18*). At trench locations on the McKinleyville and Mad River faults of the Mad River fault zone (Fig. 1), upper Pleistocene fluvial and marine terrace sediments are thrust over scarp-derived colluvium. Several ^{14}C ages from

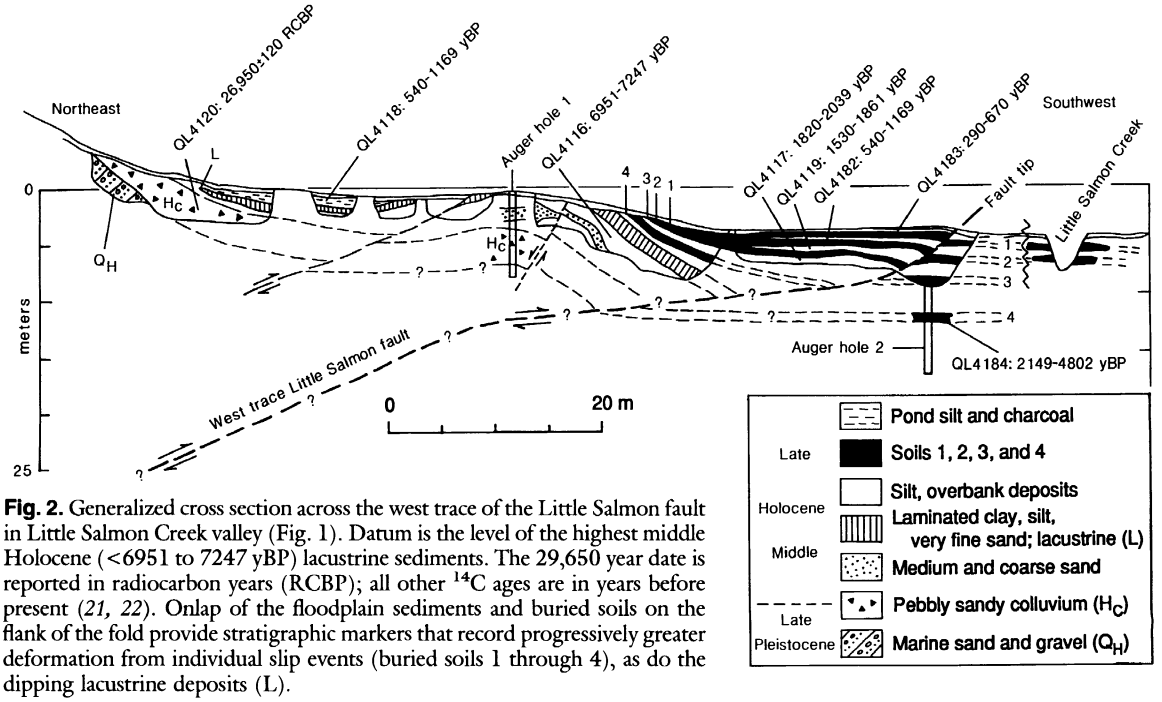

Fig. 2. Generalized cross section across the west trace of the Little Salmon fault in Little Salmon Creek valley (Fig. 1). Datum is the level of the highest middle Holocene (<6951 to 7247 yBP) lacustrine sediments. The 29,650 year date is reported in radiocarbon years (RCBP); all other ^{14}C ages are in years before present (*21, 22*). Onlap of the floodplain sediments and buried soils on the flank of the fold provide stratigraphic markers that record progressively greater deformation from individual slip events (buried soils 1 through 4), as do the dipping lacustrine deposits (L).

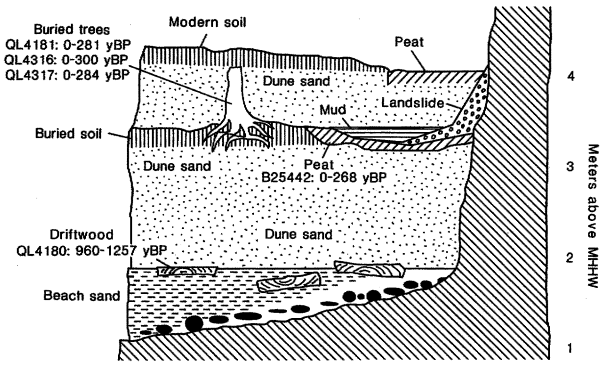

Fig. 3. Diagrammatic cross section through Holocene deposits at Clam Beach (Fig. 1). Datum is mean higher high water level (MHHW). The abrasion platform is cut into folded and faulted upper Pleistocene shallow-marine strata and is overlain by Holocene beach and dune deposits. The dune sand records two coseismic uplift events during the past 960 to 1257 years.

charcoal contained in preserved wedges of faulted colluvium beneath the overriding thrust tips indicate that both faults have experienced at least two displacement events, each resulting in at least 3.5 m of dip slip in the Holocene (*18, 20*).

Trenches across two imbricate strands of the Little Salmon fault (Fig. 1) in the Salmon and Little Salmon Creek valleys near the southeast margin of Humboldt Bay have exposed sequences of faulted and folded upper Holocene overbank floodplain deposits and buried soils. Multiple slip events are indicated by increased displacement and folding of older floodplain deposits and onlapping of younger overbank silt on the toes of the fault scarps. We found evidence for three faulting events, each resulting in 3.6 to 4.5 m of dip slip, in trench exposures on the western of the two imbricate faults (Fig. 2). Carbon-14 dating of the uppermost deformed sediments in these trenches shows that the three events occurred during about the last 1700 years; the most recent event was about 260 years before present (yBP) (*18, 21, 22*). Displacements of 1 to 2 m per event that have occurred on the smaller eastern fault strand may be synchronous with these events.

Faulted earlier Holocene sediments exposed in the trenches exhibit greater amounts of deformation. Overbank floodplain silt that has a ^{14}C age of 2149 to 4802 yBP is displaced about 18 m across the western fault (Fig. 2), and fluvial sand and gravel of similar age have been displaced at least 8 m across the adjacent eastern fault. These displacements suggest that the combined late Holocene slip rate is 6 to 12 mm/yr for the Little Salmon fault.

Raised beaches along several sections of the coast north of the MTJ provide evidence of repeated episodes of late Holocene uplift. Fossil mollusk shells from raised beaches and shore platforms at Cape Mendocino (Fig. 1), just north of the MTJ, have ^{14}C ages of 3100 to 3700 yBP (*23*). The fossil mollusk shells are in growth position, suggesting that uplift was sudden and coseismic.

A low emergent terrace, known locally as Clam Beach (Fig. 1), demonstrates that late Holocene coseismic uplift occurred along the coast north of Humboldt Bay. This terrace is bounded on the landward side by a former sea cliff about 35 m high. The shoreline angle, abrasion platform, and terrace cover sediments are exposed in stream-cut banks at the mouth of the Mad River. The shoreline angle and abrasion platform are cut into folded and faulted shallow-marine deposits of late Pleistocene age (Fig. 3) (*24*). The abrasion platform is currently about 1 m above mean high water and about 3 m above mean tide level—too high to have been formed at present sea level. This relation indicates that the terrace has been tectonically raised. The terrace cover sediments consist of a thin (1 to 2 m thick) pebbly beach sand overlain by two eolian dune sequences that are separated by a weakly developed buried soil. Driftwood collected from the beach sand directly above the abrasion surface yielded a ^{14}C age of 960 to 1257 yBP. The only source for these dune sands is the adjacent seafloor, which became emergent following sudden uplift and local regression of the shoreline. The buried soil represents weathering of the dune surface during interseismic stabilization of the dunes. Entombed in the upper dune sequence, which was probably deposited following a second episode of coseismic uplift, are trees that are rooted in the buried dunes and in peat that accumulated in back-dune hollows during the interseismic interval. The ^{14}C ages from these trees and peat range from about 250 to 300 yBP. The amount of uplift recorded at Clam Beach is not known. Because modern shoreline angles and wave-cut platforms in similar poorly consolidated sediments in this region are being cut several meters below sea level, each of the events at Clam Beach may have involved at least several meters of uplift.

Holocene coseismic subsidence is apparent from submerged and buried marshes and forests around the northern margin of Humboldt Bay. At the Mad River Slough (Fig. 1), located near the axis of the Freshwater syncline, at least four, and possibly five, stacked buried marsh or forest horizons represent the uppermost Holocene (Fig. 4) (*25*). Each horizon consists of a sequence of intertidal mud and fine sand about a meter thick that is capped by a 10- to 30-cm-thick layer of peat. The peat layers contain fossil remains of salt marsh plants indicative of uppermost intertidal and supratidal environments. Around the outer margin of the bay, the youngest of these buried marsh peats grades into buried soils containing many rooted stumps of fossil Sitka spruce. Each intertidal mud sequence rests in sharp contact with the underlying peat; such a contact is indicative of coseismic submergence. All of these salt-marsh-peat and fossil-forest horizons are within or below the modern intertidal zone.

These buried marshes and forests are similar to sedimentary sequences that are currently forming in bay margins along the coast of Alaska as a consequence of coseismic subsidence resulting from the great 1964 Alaskan subduction zone earthquake (*26*). These deposits also resemble buried marsh sequences found in several bays and estuaries along the coast of Oregon and Washington (*27, 28*) that have been interpreted as resulting from coseismic subsidence. Calibrated ^{14}C ages for the buried marsh peat layers and fossil trees in the Mad River Slough are about 250 to 300, 950 to 1250, 950 to 1350, and 1450 to 1650 yBP (Fig. 4); an additional weakly developed and locally absent peat beneath the upper

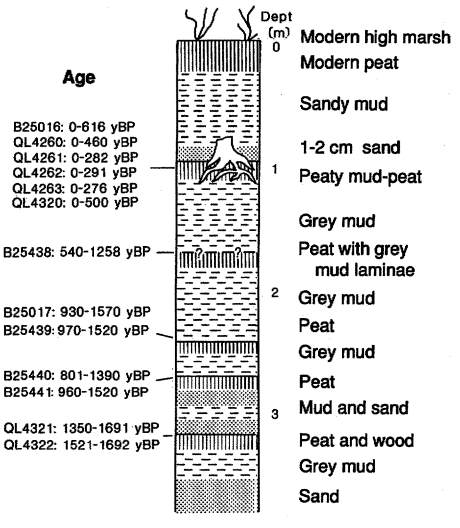

Fig. 4. Composite stratigraphic column through late Holocene deposits at Mad River Slough (Fig. 1). Datum is the modern high marsh surface. Intertidal mud (dashed) that abruptly overlies marsh peat (vertical lines) indicates abrupt, episodic submergence at four or five different times during the past 1423 to 1690 years. Each submergence probably resulted from coseismic subsidence.

buried horizon has been dated at about 550 to 1250 yBP. Several of these ages correspond (within standard errors) to the events identified at Clam Beach and on the Little Salmon fault (Fig. 5).

We thus infer that the SCSZ is active, that major thrust faults in the accretionary prism are genetically related to the subduction process, and that late Holocene displacement, uplift, and subsidence are associated with two such zones of faulting, the Little Salmon fault and the Mad River fault zone. The magnitude and distribution of deformation are similar to those observed from great historic subduction zone earthquakes in Japan (*3*), Alaska (*29*), and Chile (*30*), and suggest that the SCSZ has repeatedly produced large subduction earthquakes during the Holocene. These inferences permit estimates to be made of the magnitudes of these paleoseismic events.

Measurements of stratigraphically bracketed slip on the west trace of the Little Salmon fault and ^{14}C dating of bracketing layers indicate that the fault has generated at least three large surface displacements (3.6 to 4.5 m per event) during the past 1700 years and has an average late Holocene slip rate of about 7 mm/yr. The east fault strand, located a few hundred meters from the west strand, has produced surface displacements of about 1 to 2 m per event that may be synchronous with these three events and has an average late Holocene slip rate of about 2 to 3 mm/yr. Combined, surface displacements on both strands have been as much as 4.6 to 6.5 m per event. The recurrence interval is 300 to 560 years, and the late Holocene slip rate is 6 to 12 mm/yr. The fault has a length of about 100 km, and we estimate that the area of the related earthquake-producing rupture surface is about 4000 km^2. Regression relations between magnitude and rupture length, surface displacement, and recurrence interval and slip rate (*31*) suggest that the magnitudes for these events would have been at least $M_s \approx 7.6$. Relations between rupture area (A = 4000 km^2) and magnitude [M = log A + 4.15 (*32*)] suggest that magnitudes were about 7.8.

Two lines of reasoning suggest that the Little Salmon fault moved during larger megathrust events and that these magnitudes are too low. Half or more of the convergence between the Gorda and North American plates, estimated at 30 to 40 mm/yr (*2*), is apparently expressed as compressional deformation across the North American plate margin (*5*). Earthquakes yielding average late Holocene slip of 6 to 12 mm/yr (Little Salmon fault zone) and 5 to 7 mm/yr [Mad River fault zone (*5*)] would relieve only part of the convergence-related elastic strain. The remainder must be relieved by displacements on other faults, as yet unidentified by field and seismicity studies, or by displacement on the underlying SCSZ megathrust. Second, similar thrust faulting in accretionary prisms elsewhere is commonly in direct response to movement on the underlying subduction zone (*3*). Hence, we suspect that movement on the Little Salmon and Mad River fault zones is associated with large paleoseismic events on the CSZ megathrust.

If the CSZ is segmented, rupture on the SCSZ megathrust between the Blanco fracture zone and the MTJ (Fig. 1) would be approximately 240 km long and 70 to 80 km wide. We estimate this width by assuming that rupture would extend seaward to the western limit of strong coupling between the Gorda and North American plates (SD in Fig. 1) (*7*) and landward to where the dip of the downgoing plate increases from ~11° to ~25° (*8, 33*). This area corresponds to the region of shallow crustal seismicity, which is the region between the seismic and aseismic fronts (*34*) in the accretionary margin of the North American plate. The resulting rupture area—about 17,000 to 19,000 km^2—would correspond to an earthquake of magnitude 8.4 (*32*).

If elastic strain is accumulating along the entire length of the CSZ (1200 km), events as large as the 1960 Chilean earthquake (M_w = 9.5), which ruptured an area of similar dimension, may be possible (*3*). Large subduction zone ruptures elsewhere have been known to propagate across apparent structural boundaries, such as fracture zones in the subducting plate (*3*). Furthermore, comparison of the ages of paleoseismic evidence from central Washington to northern California (*27, 28, 35–37*) shows that much or all of the CSZ has ruptured within time intervals shorter than the range of uncertainties for the ^{14}C age estimates. This suggests that either events on CSZ segments have been temporally clustered, or long parts of the subduction zone have ruptured in single giant earthquakes.

Although the seismic potential of the CSZ is not yet resolved, the preponderant geologic evidence now supports the interpretation that great subduction-related earthquakes have occurred in this region in the recent past and presumably will recur in the future. Our studies indicate that maximum events in the 7.6 to 7.8 magnitude range are less probable than those having magnitudes in the range of 8.4 or larger. Characterization of these earthquakes, particularly with respect to recurrence interval and structural segmentation of the CSZ, is vital because subduction zone earthquakes of the magnitudes suggested are well known to generate extensive damage from ground shaking, liquefaction, ground failure, and large tsunamis.

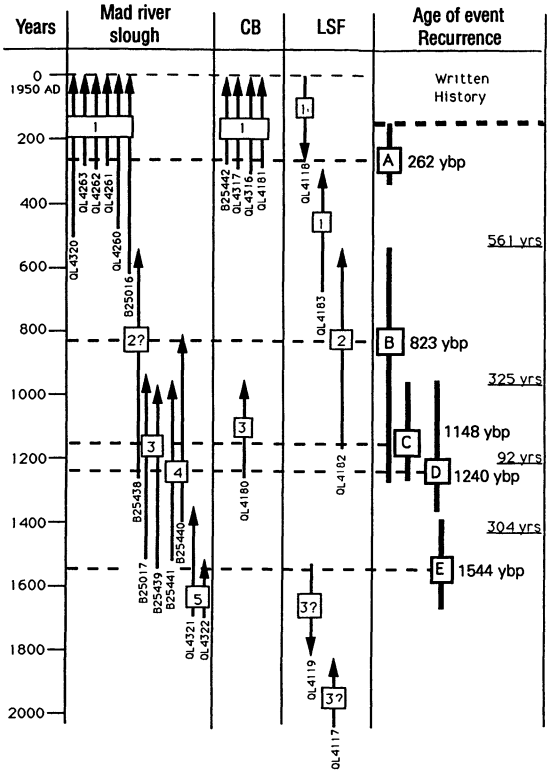

Fig. 5. Summary chart showing age estimates and recurrence intervals for late Holocene paleoseismic events from the Humboldt Bay region. Dashed lines show averages of the most probable calibrated ages (*26, 27*) of individual events. Lengths of arrows indicate 2σ calibrated age determinations for individual events. Upward directed arrows are maximum limiting ages. Downward directed arrows are minimum limiting ages. Numbered boxes refer to the stratigraphic positions of paleoseismic horizons at the localities specified. Carbon-14 age estimates for paleoseismic events at the three sites discussed provide a preliminary chronology for five large earthquakes (A through E) during the past 1690 years, with recurrence intervals ranging from 92 to 561 years. The most recent event occurred about 150 to 277 yBP, with the most probable age about 260 yBP.

REFERENCES AND NOTES

1. M. Ando and E. I. Balazs, *J. Geophys. Res.* **84**, 3023 (1979).
2. T. H. Heaton and H. Kanamori, *Seismol. Soc. Am. Bull.* **74**, 933 (1984).

3. T. H. Heaton and S. H. Hartzell, *ibid.* **76**, 675 (1986).
4. S. H. Clarke, Jr., *Geol. Soc. Am. Abstr. Progr.* **20**, A382 (1988).
5. G. A. Carver, in *Tectonics, Sedimentation, and Evolution of the Eel River and Other Coastal Basins of Northern California*, H. Schymiczek and R. Suchland, Eds. (*San Joaquin Geol. Soc. Misc. Publ.* **37**, San Joaquin Geological Society, Bakersfield, CA, 1987), pp. 61–72.
6. S. H. Clarke and M. E. Field, in *California Continental Margin Geologic Map Series*, H. G. Greene and M. P. Kennedy, Eds. (*Map No. 7A, Geology*, California Division of Mines and Geology, Sacramento, 1989).
7. S. H. Clarke, Jr., *Am. Assoc. Petrol. Geol. Bull.*, in press.
8. R. C. McPherson, thesis, Humboldt State University, Arcata, CA (1989).
9. H. M. Kelsey and G. A. Carver, *J. Geophys. Res.* **93**, 4797 (1988).
10. G. A. Carver, R. M. Burke, H. M. Kelsey, *U.S. Geol. Surv. Open-File Rep. 86-31*, 58 (1985).
11. _____, *Geol. Soc. Am. Abstr. Progr.* **18**, 93 (1986).
12. M. Lisowski and W. H. Prescott, *Eos* **70**, 1332 (1989).
13. M. L. Zoback, *U.S. Geol. Surv. Open-File Rep. 88-16* (1988), p. 544.
14. D. S. Wilson, *J. Geophys. Res.* **94**, 3065 (1989).
15. T. Atwater, *Geol. Soc. Am. Bull.* **81**, 3513 (1970).
16. D. C. Engebretson, A. Cox, R. G. Gordon, *Geol. Soc. Am. Spec. Pap. 206* (1985).
17. G. A. Carver and R. M. Burke, *Geol. Soc. Am. Abstr. Progr.* **19**, 614 (1987).
18. _____, *Final Report, National Earthquake Hazards Reduction Program* (U.S. Geological Survey, Menlo Park, CA, 1988).
19. G. S. Vick and G. A. Carver, *Geol. Soc. Am. Abstr. Progr.* **20**, A232 (1989).
20. G. A. Carver, *U.S. Geol. Surv. Open-File Rep. 87-673* (1987), p. 115.
21. M. Stuiver and G. W. Pearson, *Radiocarbon* **28**, 805 (1986).
22. Carbor-14 ages are calibrated as calendar years before A.D. 1950, and were calculated using a microcomputer program obtained from the Quaternary Isotope Laboratory of the University of Washington [M. Stuiver and P. J. Reimer, *Radiocarbon* **28**, 1022 (1986)]. Laboratory error multipliers used are 1.6 for QL (Quaternary Isotope Laboratory of the University of Washington) and 2.0 for B (Beta Analytic, Inc.). Only 2σ (95% confidence level) calibrated age ranges are reported.
23. K. R. Lajoie, A. M. Sarna-Wojcicki, Y. Ota, *Geol. Soc. Am. Abstr. Progr.* **14**, 178 (1982).
24. G. Berger, R. M. Burke, G. A. Carver, D. J. Easterbrook, *Chem. Geol.* **87**, 21 (1991).
25. G. S. Vick, thesis, Humboldt State University, Arcata, CA (1989).
26. A. T. Ovenshine, D. E. Lawson, S. R. Bartsch-Winkler, *J. Res. U.S. Geol. Surv.* **4**, 151 (1976).
27. B. F. Atwater, *Science* **236**, 942 (1987).
28. M. E. Darienzo and C. D. Peterson, *Tectonics* **9**, 1 (1980).
29. G. Plafker, *Science* **148**, 1675 (1965).
30. _____ and J. C. Savage, *Geol. Soc. Am. Bull.* **81**, 1001 (1970).
31. D. B. Slemmons and C. M. Depolo, in *Active Tectonics* (National Academy Press, Washington, DC, 1986), pp. 45–62.
32. M. Wyss, *Geology* **7**, 336 (1979).
33. R. S. Cockerham, *Seismol. Soc. Am. Bull.* **74**, 569 (1984).
34. D. E. Byrne, D. M. Davis, L. Sykes, *Tectonics* **70**, 833 (1988).
35. W. C. Grant *et al.*, *Eos* **70**, 1331 (1989).
36. J. Bourgeois and M. A. Reinhart, *ibid.*, p. 1331.
37. J. Adams, *Tectonics* **9**, 569 (1990).
38. We are grateful to B. F. Atwater and G. Plafker for their thoughtful reviews of the original manuscript. Paleoseismicity investigations have benefited from support by U.S. Geological Survey National Earthquake Hazards Reduction Program grant number 14-08-0001-G1082 and National Sea Grant number NA89AA-D-SG138.

22 July 1991; accepted 19 November 1991

GAP Domains Responsible for Ras p21–Dependent Inhibition of Muscarinic Atrial K^+ Channel Currents

GEORGE A. MARTIN, ATSUKO YATANI, ROBIN CLARK, LEAH CONROY, PAUL POLAKIS, ARTHUR M. BROWN, FRANK MCCORMICK

The interaction between the low molecular weight G protein ras p21 and a guanosine triphosphatase activating protein (GAP) uncouples a heterotrimeric G protein (G_k) from muscarinic receptors. Through the use of isolated atrial cell membranes and genetically engineered GAP deletion mutants, the src homology regions (SH2-SH3) at the amino terminus of GAP have been identified as the domains responsible for this effect. Deletion of the domain required to stimulate the guanosine triphosphatase activity of ras p21 relieves the requirement for ras p21 in this system. A model is presented that suggests that ras p21 induces a conformational change in GAP, which allows the SH2-SH3 regions of GAP to function.

THE SIGNALING PATHWAY BETWEEN atrial muscarinic (M2) cholinergic receptors, heterotrimeric G proteins (G_k, probably G_{i2} or G_{i3}), and single muscarinic K^+ channels (K^+[ACh]) can be interrupted in vitro by ras p21 or one of its guanosine triphosphatase (GTPase) activating proteins (GAPs) (*1*). Interruption occurs by uncoupling of the receptor from the G protein rather than uncoupling of the G protein from the channel. The biochemical basis of the effect is not yet understood, but it serves as a sensitive assay for ras p21 and GAP function in a cell-free system. The function of ras p21 depends on interaction with GAP, and vice versa, suggesting that a functional complex forms between these two proteins and that this complex is responsible for interrupting the muscarinic signaling pathway (*1*).

GAP interacts with a number of proteins in vitro. A COOH-terminal domain is responsible for binding H-ras, N-ras, K-ras, and R-ras p21 proteins and for stimulating their GTPase activities (*2*). This domain also binds tightly to the product of the *K-rev1* gene, rap1A p21, but in this case no stimulation of GTPase activity occurs (*3*). GAP binds to phosphoproteins, such as platelet-derived growth factor (PDGF) and epidermal growth factor (EGF) receptors, v-src, and two unidentified phosphoproteins referred to as p190 and p62 (*4–9*). These interactions are mediated by the SH2 regions of GAP (*10, 11*). GAP therefore has the ability to bind two classes of signaling proteins, ras p21 proteins and phosphoproteins, and may serve as a functional link between these signaling pathways. We have now used genetically engineered GAP mutants to identify the GAP domains required for the ras-dependent inhibition of muscarinic receptor coupling to G_k.

The structures of the mutant GAPs used are shown in Fig. 1. GAP17 contains the complete coding sequence of human type I GAP (*12*), the major species of GAP expressed in most tissues (*13*). Three domains are of particular interest: (i) the NH_2 terminus, which contains a hydrophobic region of about 180 amino acids (*12*); (ii) the SH2-SH3 domains, regions of homology with regulatory sequences of non-receptor tyrosine kinases, phospholipase C-γ, the p85 subunit of PI 3′ kinase, and the crk proto-oncogene (*14–19*); and (iii) the catalytic domain, the region sufficient to stimulate ras p21 GTPase activity (*2*). At the COOH-terminus of each GAP mutant, eight amino acids corresponding to the COOH-terminus of SV40 T-antigen were added to facilitate purification of recombinant proteins by the KT3 monoclonal antibody (*20*). GAP16 corresponds to type II GAP, a splicing variant expressed at high concentrations in human placental tissue (*12, 13*). This protein lacks the hydrophobic NH_2-terminus characteristic of type I GAP but is otherwise identical.

The ability of these affinity-purified proteins and of the truncated derivatives (Fig. 1) to inhibit K^+[ACh] currents was tested as described (*1, 21*). The efficiency of full-length type I GAP, which contains the KT3 epitope, was compared with the GAP preparation used in the previous study. The proteins were equally efficient in preventing receptor-mediated channel opening (data not shown). In

G. A. Martin, R. Clark, L. Conroy, P. Polakis, F. McCormick, Department of Molecular Biology, Cetus Corporation, Emeryville, CA 94608.
A. Yatani and A. M. Brown, Department of Molecular Physiology and Biophysics, Baylor College of Medicine, Houston, TX 77030.